BOLLETTINO DI GEOFISICA TEORICA ED APPLICATA VOL. 39, N. 3, pp. 181-198; SEPTEMBER 1998

Numerical modelling assisted analysis of the seismic image of a brine-filled cavity

F. COREN, E. PRIOLO, A. PREGARZ, S. PERSOGLIA and G. PADOAN

Osservatorio Geofisico Sperimentale, P.O. Box 2011, 34016 Trieste, Italy

(Received December 15, 1997; accepted May 26,1998)

Abstract. A seismic survey was carried out in the area of a salt mine area with the principal aims of identifying potential zones of subsidence, and the locations and sizes of the water filled cavities generated during salt extraction. Several high resolution 2-D seismic profiles were acquired and interpreted, allowing a detailed definition of the main stratigraphic units as well as the general geological setting. However, cavity identification and location remained uncertain. For improving the interpretation, a 2-D model was developed in order to characterize the seismic signature of these cavities. The model represents the cross-section of a brine filled cavity imbedded in a two layer half-space, and reproduces the situation at a site which was well known from well data and sonar investigation. Wave propagation was simulated by solving numerically the scalar full wave equation with the Chebyshev spectral element method. The dynamics of this model, as well as the analysis and characterization of the seismic signature of the cavity in a stacked section, are illustrated and explained in the paper. Synthetic results are directly compared with the real data, and a critical analysis of the detectability of water-filled cavities is given. Among the results, it was observed that reflection and diffraction from the cavity bottom is stronger than that from the cavity top; however, the diffraction hyperbolas from cavity top and bottom, which would usually be the strongest evidence for the presence of a cavity, may often be hidden in real data by seismic noise, making detection difficult. Finally, a further seismic stacked section acquired at a different site is discussed in the light of the experience acquired.

1. Introduction

The Belvedere Spinello salt mine is located in southern Italy near the town of Crotone (Fig. 1a). The deposit consists of a 250 m thick sequence of halite rock interbedded with thin layers

Corresponding author: E. Priolo, Osservatorio Geofisico Sperimentale, P.O. Box 2011, 34016 Trieste, Italy; Tel.: +39 040 2140 351; Fax.: +39 040 327521; e-mail: epriolo@ogs.trieste.it

of clastic origin. The halite formation is underlain by a continuous anhydrite layer.

Extraction of the salt is done by a solution-mine technique (Barnes, 1988), in which large volume chambers are developed underground. Control of the location, shape and dimension of such cavities, and consequently of the pillars between them, guarantees the geotechnical stability of the site. The 2-D seismic survey was conducted in the area with a threefold aim: i) of detecting the presence of cavities imbedded in the salt formation and evaluating the possibility of collapse; ii) of tuning the acquisition parameters in preparation for a 3D high resolution seismic (HRS) survey; iii) of improving geological and geotechnical knowledge at the site.

During the interpretation of the 2D-HRS lines for searching for cavities, it turned out that an accurate understanding of the seismic response of such a system was needed. In general, the possibility and effectiveness of detecting underground cavities by surface seismics is an interesting topic in many geotechnical, environmental and archaeological applications (Branham and Steeples, 1988; Miller and Steeples, 1995). Numerical modelling of the seismic wave propagation can play an important role when interpreting real data.

In view of the scarcity of papers tackling this topic through the use of synthetics, a recent paper by Bruno and Rapolla (1997) deserves mention, in which numerical modelling of the 2-D scalar wave equation was used to predict the seismic response of a ground-cavity system. The synthetics of the numerical models were the main reference in the interpretation of some reflection seismic lines. Moreover, the paper mentioned various processing techniques for searching for the diffraction hyperbola generated by the cavities, and for any breaks in seismic reflectors below them. The seismic surveys were carried out at two test sites in an urbanized area characterized by volcanic rocks, whose shallow part consists of incoherent and dry pyroclastic material which gives strong attenuation. Field data were characterized by a high noise level (for instance due to ground roll, and the presence of building foundations and concrete basements) that made it hard to identify and separate the effects of a single event.

Also in our case modelling proved to be an essential tool for the interpretation, helping us to exactly identify the seismic features related to the presence of the cavities. In the present study, we compute numerically the stacked seismic section for an acoustic wave propagation through a model reproducing the real situation beneath one of the wells. Looking at the propagating waves we discuss the physics and identify events due to the cavity, the main aim being to provide an interpretation key to cavity signatures in stacked sections. Comparison of synthetics with real data shows an excellent agreement, taking account of environmental noise. Finally, in the light of experience acquired, we analyse the seismic sections for detecting other cavities.

2. Geological setting of the area

The Belvedere Spinello salt mine (Fig. 1) is located within the thick sedimentary sequence of the northern Crotone Basin. The basin stratigraphy records a strong regressive phase during the Middle Miocene, followed by an evaporitic cycle. A series of anhydrite layers indicates the

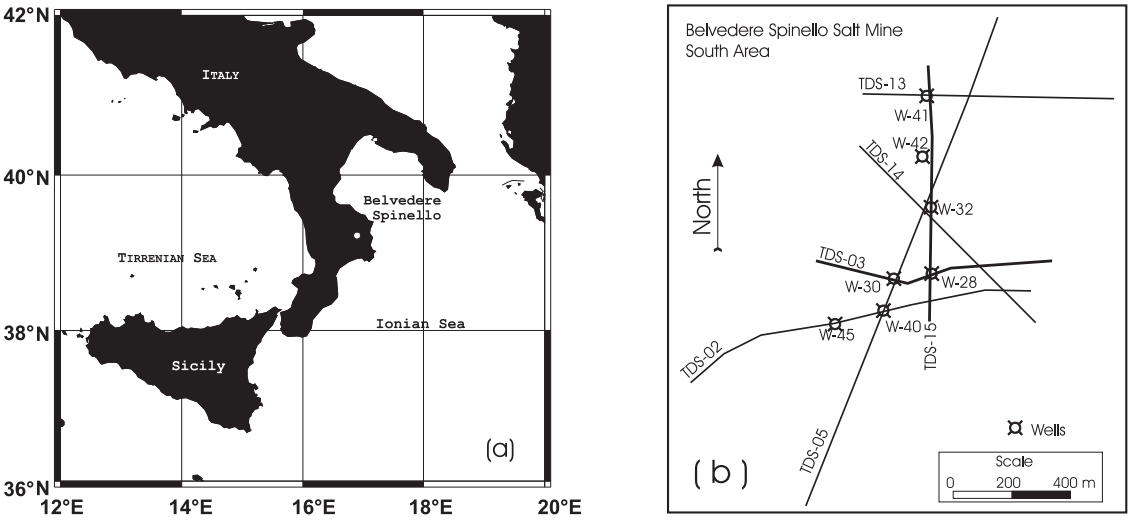

Fig. 1 - a) Geographic framework of the study area. b) Position map of the southern area, containing the 2D-HRS lines and location of wells . TDS-03 and TDS-15 (thick lines) are the profiles analysed in this work.

beginning of the cycle, whereas its advance is recorded by deposition of the Lower Evaporite formation salt bank . The climax is reached with the deposition of the Detrital-Saline formation; and the relaxation phase gave the Upper Evaporite formation. Both are constituted by salt. Subsequently, an abrupt change in paleoenvironmental conditions occurred, as recorded by a clastic unit (Carvane conglomerate), which represents both the top of the Messinian evaporitic cycle and the base of the Pliocene Transgression. The subsequent ingression of the sea produced a coast and lagoon bar in the area. These two etheropic formations are respectively the Scandale sandstone and the Spartizzo marly clay. At this stage a rise in the sea level determines the beginning of a different sedimentation pattern, characterized by a larger fraction of clay and silt (Cutro formation) (Roda, 1964).

The Lower Evaporite, Detrital, and Upper Evaporite formations form the halite ore deposit, the objective of the mining. In the restricted area of the survey, not all the above described units are present, in particular along lines TDS-03 and TDS-15 (see Fig. 1b). The geological interpretation of the seismic sections was done using the stratigraphic information derived from the wells. This allowed identification of the units as indicated in Table 1. The same table also shows the cross-reference to the seismic model.

3. Survey methodology and targets

The mining area of Belvedere-Spinello can be divided into two zones. The northern defines the former extraction zone where the old *multiple-well* solution mine technique (SMT) was adopted, with no sonar control. In the southern area (Fig. 1b), currently the active zone, mining is

Table 1 - Geological units identified by the interpretation of the seismic lines and their correlation with the model.

Real units	Model reference
Weathering layer 8 - 15 m	
Cutro Marly Clay Scandale Sandstones Spartizzo Marly Clay	SEDIMENTARY SEQUENCE
Upper Evaporite formation Detrital Saline formation	SALT LAYER

performed using the modern *single-well* SMT, and includes sonar monitoring of the growing cavities.

With the latest technique, a single hole is drilled to the bottom of the salt layer. Then, two concentric tubes are introduced into the hole, the inner one reaching the lowest part of the salt layer, and the external one being some tens of meter higher. Water is then pumped into the inner tube and flows out through the external, dissolving the salt formation. The lateral extent of the cavities is controlled by a *blanket*: an injection of either nitrogen or light hydrocarbons into the cavity. In practice, the blanket prevents the dissolution of the top of the cavity, thus allowing its lateral expansion. The final result of mining activity is a series of large cavities (approximately 200 000 cubic meters in volume each) filled by salty water and distributed over a semi-regular grid, as in the conventional chamber and pillar mining technique (Barnes, 1988). The pillars of the undissolved salt between the cavities assure the stability of the mining site.

With the old multiple-well SMT, not only was cavity location difficult to control, but also dimension and lateral expansion, thus creating potential collapse zones. This was one of the main concerns in the former mining zone A.

For the reasons given above, a 2D-HRS survey was proposed with the principal targets of identifying the locations of the underground cavities and investigating the presence of potential collapse zones. This survey was funded partly by the UE under the project "High Resolution 3-D Seismic Reflection Applied to Subsidence Evaluation and Solution Mine Design" (HIRES-SESOM BE-5889), and partly by Montecatini S.p.A.. In addition to the main targets, the survey provided a test for finely tuning acquisition parameters in view of a more expensive 3-D HRS survey. The main tasks of the project were: the construction of a geological model; characterization of the entire deposit by extending local information from the wells; identification of any possible underground collapse structures and potential area of subsidence; and location and characterization of the cavities.

The acquisition of the 2D-HRS lines was done with a telemetric digital seismic recorder SERCEL SN-348. The energy source was dynamite, which provided energy over a broad frequency range (up to 150 Hz, with a dominant frequency of 50-60 Hz); the charges (approx. 350 g/shot) were inserted into 12 m deep holes. The acquisition parameters were varied from line to line in order to achieve the optimal configuration for the planned target. Table 2 lists the parameters adopted for the lines TDS-03 and TDS-15. However, only a few variations were needed

Table 2 - Recording parameters of the lines TDS-03 and TDS-15. Bold indicates different settings.

	TDS-03	TDS-15
recorder	SERCEL SN-348	SERCEL SN-348
data format	SEG-B	SEG-B
density	6250 BPI	6250 BPI
number of channels	96	96
trace interval	10 m	6 m
converge	1200%	1200%
record length	3 s	2 s
sampling	1 ms	1 ms
geophone frequency	10 Hz	10 Hz
geophone pattern	rectangular	rectangular
patern length	18,25 m	11 m
geophone interval	1.66 m	1.00 m
number of geophones per trace	12	12
recording geometry	ASYMETRICAL SPLIT	ASYMETRICAL SPLIT
number of shot holes	1	1
charge depth	10 - 12 m	10 - 12 m
charge quality	100 - 200 g	100 - 200 g
shotpoint interval	40 m	24 m
recording filters	LC 10 Hz - HC 250 Hz	LC 10 Hz - HC 250 Hz
Notch filter 50 Hz	OUT	OUT

in the acquisition parameters, mainly in trace and shotpoint interval.

4. Modelling and interpretation

4.1. Interpretation uncertainties

The high quality of the 2-D HRS seismic data allowed an accurate interpretation of the underground structure. Fig. 2 shows the geological and structural setting of the area and the main interpreted stratigraphic units. The geological units were interpreted on the seismic section only by correlation with the stratigraphy derived from the wells; no logs were available. Check-shots and stacking velocities were used to compute time-depth relationships between wells and seismics. However, in order to clearly detect the presence of cavities we needed to understand the characteristics of their signature in a stacked seismic section. A further problem in dealing with stacked data was that the diffraction hyperbola were often hidden by other effects (for instance, material inhomogeneities, anisotropy, and lithological changes) or might be mistakenly identified with similar events of other origin (such as dome-shaped structures within the salt formation; for instance, the wide hyperbola in Fig. 2 at time 0.40-0.45 s between wells 43 and 28). These “spurious” phenomena obviously prevented a reliable recognition of the cavity pattern in the real data.

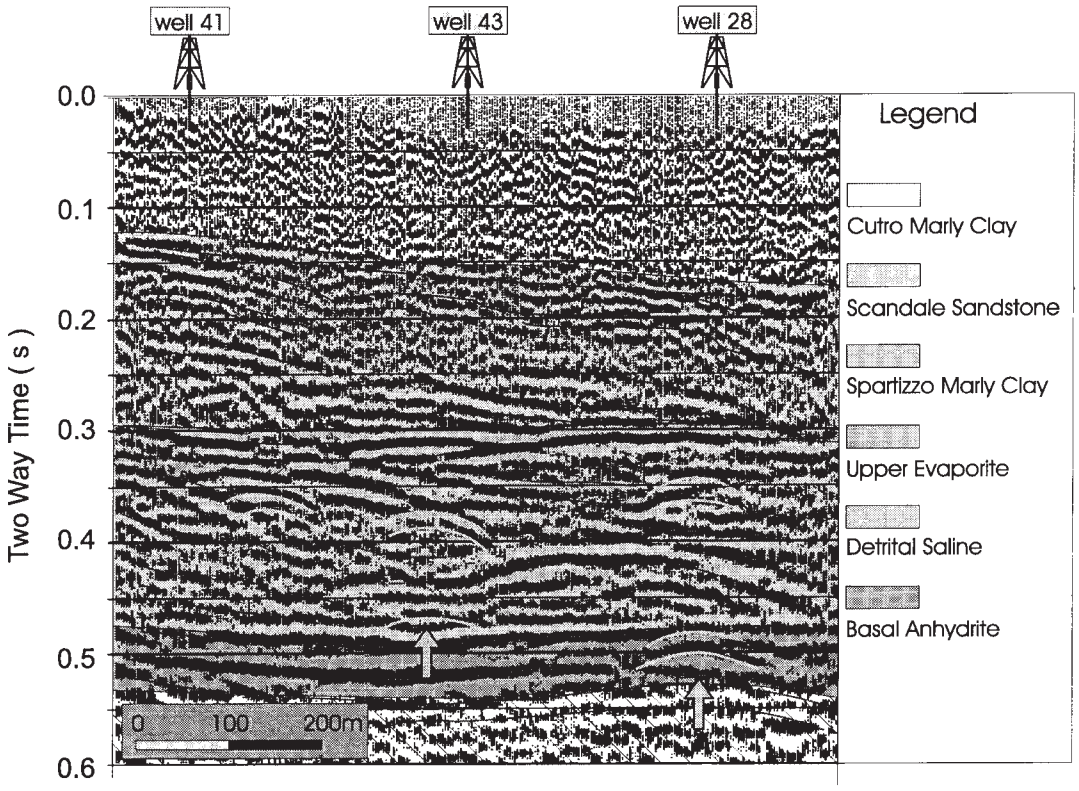

Fig. 2 - Interpreted zero-phase stacked seismic line TDS-15. The geological intrerpretation as well as the line drawing are represented. Thin continuous red lines mark main reflectors. Thick yellow lines define hyperbolic diffractions that were related to the presence of cavities in the light of the numerical simulation. Yellow arrows indicate the pull down effect in the layers located beneath the cavities.

4.2. Modelling the cavity response

To obtain an accurate interpretation along the 2-D HRS lines and study the seismic behavior and signature of the cavity in real data, a model solving the scalar wave equation has been developed. The solution was computed numerically by the Chebyshev spectral element method (SPEM). A brief description of this method is given in Appendix 1.

CAVITY MODEL. - We chose well 28 as test site, because here we have a realistic model of both the stratigraphy and the underlying cavity morphology. Moreover, the well is situated at the intersection of two seismic lines (TDS-03 and TDS-15; Fig. 1b).

The model (Fig. 3) consists of two-layers with a soft inclusion simulating the cross-section of the water-filled cavity. The upper layer simulates the clastic formation (sandstone), for which the velocity corresponds to an average value of the formation. The deeper layer simulates the salt formation, which completely surrounds the brine-filled cavity. The location and shape of the cavity were reconstructed using 3-D sonar logging. This system is based on directional sonic

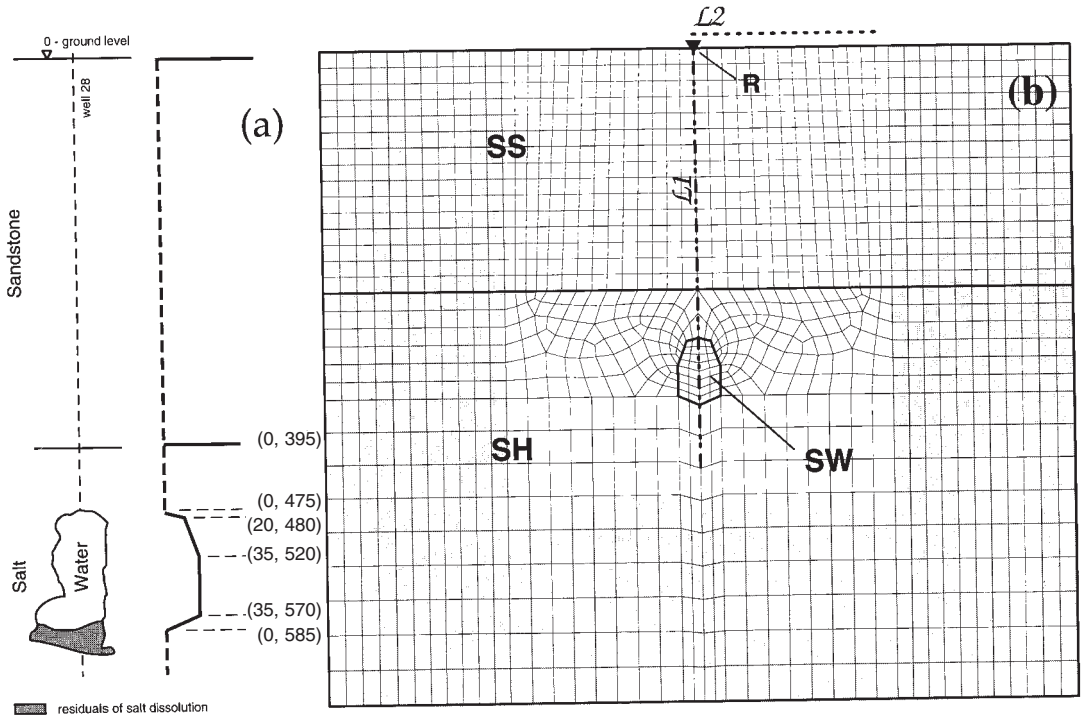

Fig. 3 - Model description. (a) Cavity profiles reconstructed from sonic log measurements (left side), and the derived synthetic profile (right side; x and z coordinates are in metres). (b) Irregular mesh used for the numerical simulation. Dashed lines indicate the two lines of receivers (L1 and L2). Materials are labelled according to Table 3. Model dimensions are specified in the text. The grey area defines the strips used to attenuate the outgoing wavefield.

measurements and provides a complete 3-D mapping of the cavity with a vertical sampling interval of 2 m and angular binning (on the horizontal plane) of about 1 degree. The 2-D cavity profile (Fig. 3a) was the simplified slice of the 3-D data along the vertical plane of the seismic line.

Material parameters are shown in Table 3. Depths are 395 m at the sandstone/salt interface, 475 m at the cavity top, and 585 m at its bottom; the maximum halfwidth of the cavity is 35 m. The resulting computational model and mesh are shown in Fig. 3b. The model size is 1240 m $\times$ 1070 m; the mesh consists of 1472 quadrangles, with polynomial order N = 6, corresponding to a total of 53449 nodes. The discretisation is irregular in order to correctly reproduce the cavity edge, and locally fits the number of grid nodes to the wavelength value, needed for an accurate solution. The free surface condition is imposed at the top of the model. A non-reflec-

Table 3 - Material description.

Material	Symbol	ρ (kg/m^3)	V_P (m/s)
Sedimentary sequence	**SS**	2450	2400
Salt (Halite)	**SH**	2170	3500
Salty water	**SW**	1200	1600

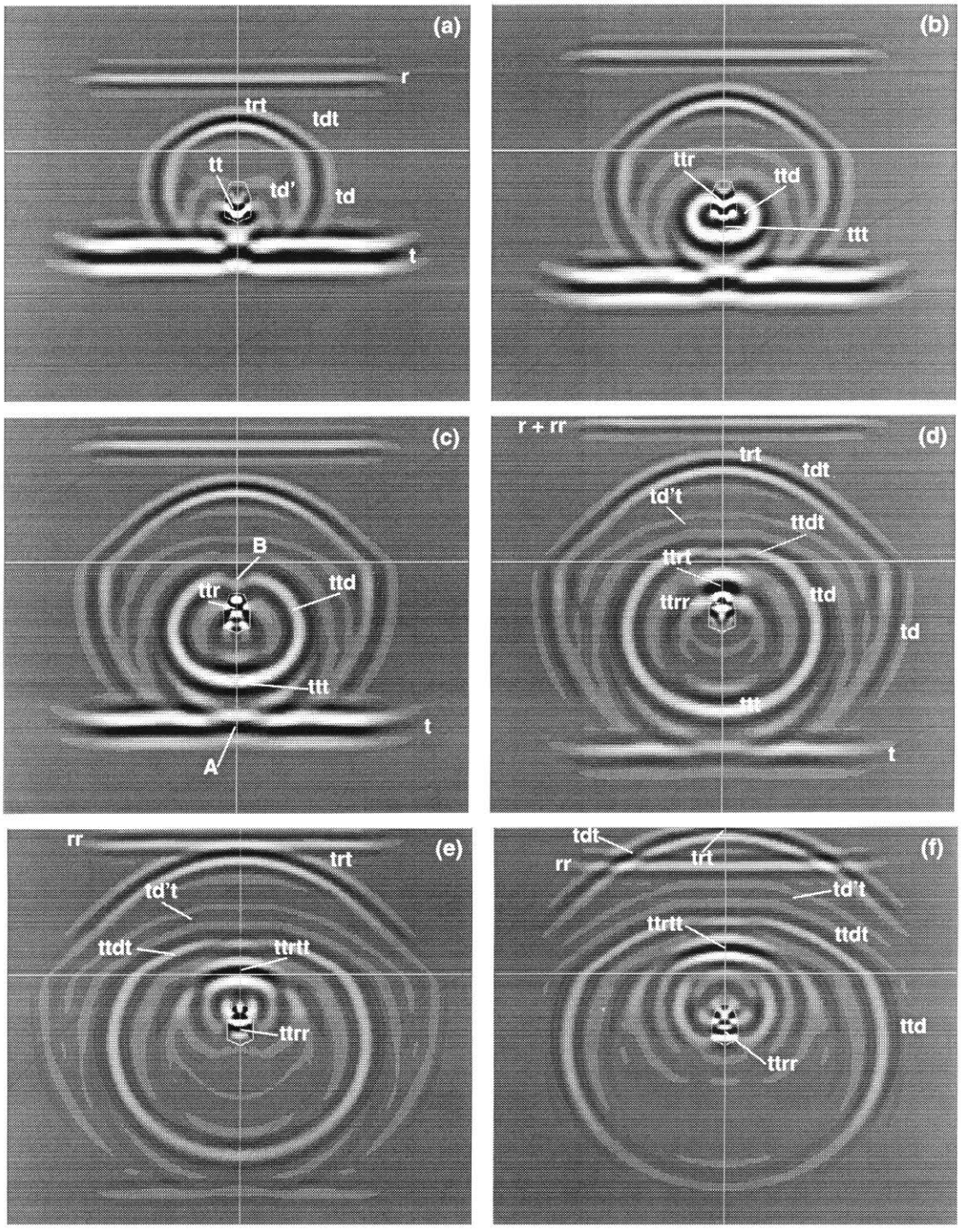

Fig. 4 - Snapshots of the displacement field at propagation times (a) 201 ms , (b) 226 ms, (c) 251 ms, (d) 276 ms, (e) 301 ms, and (f) 326 ms. Wavefronts are labeled according to the text.

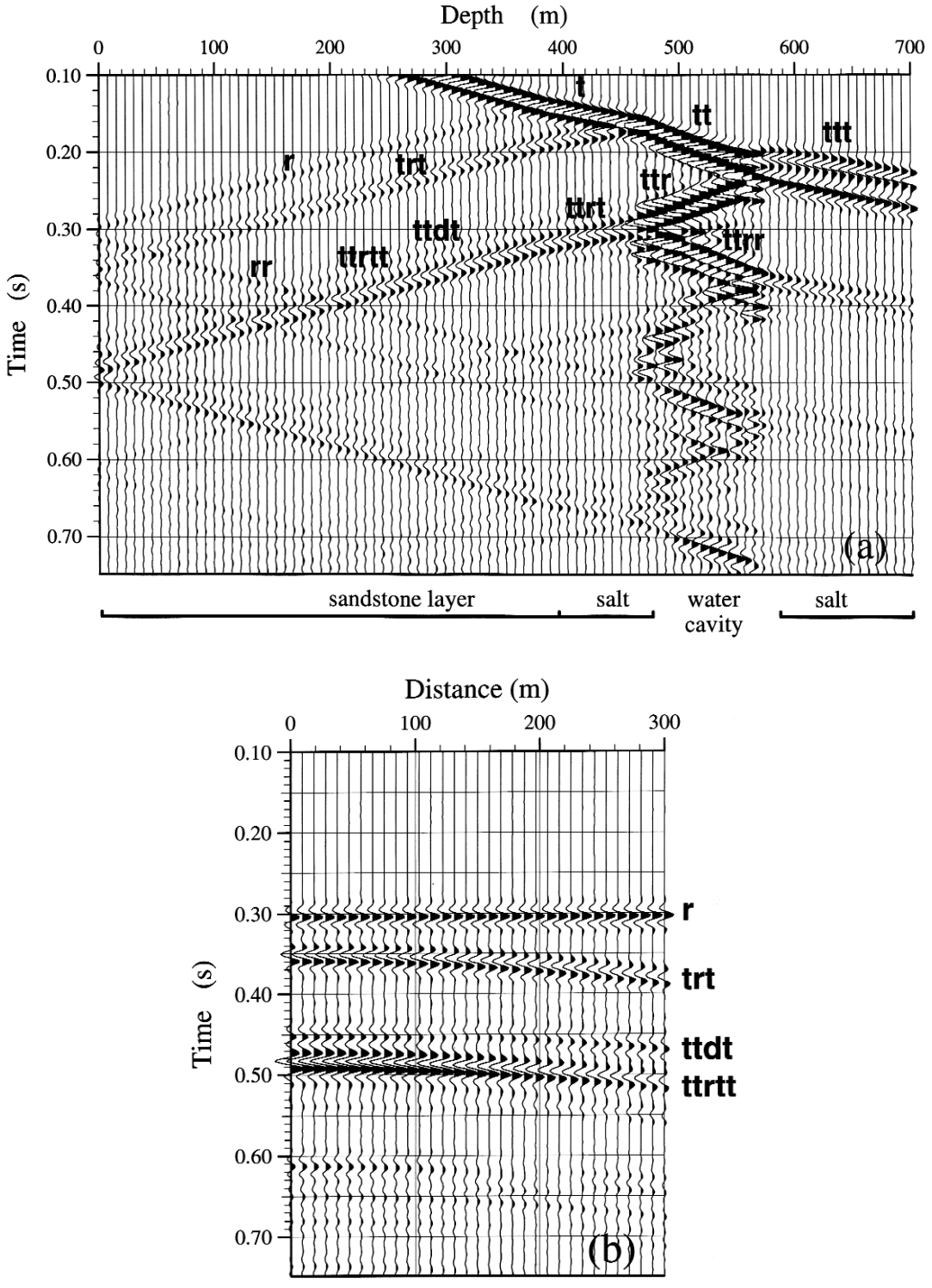

Fig. 5 - Seismograms recorded at the surface and along the vertical symmetry axis of the model (respectively (a) lines *L1* and (b) *L2* in Fig. 3b).

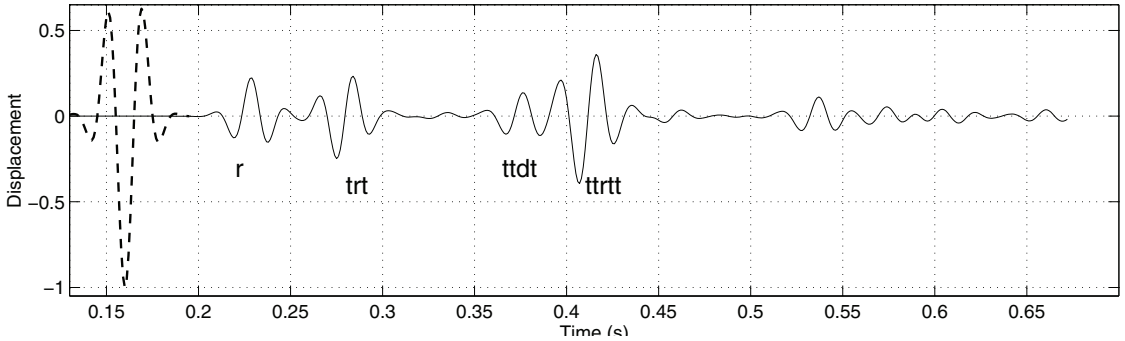

Fig. 6 - Seismogram recorded at the surface over the cavity vertical axis (receiver R in Fig. 3b). The dashed line represents the time history of the incident wave recorded at a receiver located within the sandstone layer (SS).

ting condition for the outgoing wavefield is imposed at external boundaries through an absorbing strip where the wavefield is smoothly attenuated (shaded area in Fig. 3b). No attenuation is imposed on the propagating wavefield. The computational time step is 0.625 ms; output data are sampled at 2.5 ms. The source is a pressure plane wave propagating downwards, and is initiated through two properly shifted plane wavefronts. The central frequency is 50 Hz.

MODELLING RESULTS AND INTERPRETATION. - Fig. 4 and Fig. 5 show snapshots of the acoustic field at six different propagation times and seismograms at the surface and along the vertical symmetry axis of the model (receiver lines *L2* and *L1*, respectively).

In the first snapshot (Fig. 4a) the propagating plane wave has just been transmitted through the cavity. The downgoing transmitted direct wave (t) and the upgoing first layer multiple (r) are easily identified. Then, the following phases can be seen [2] : trt is the first reflection of the cavity top, which propagates upwards through the sedimentary layer. This wavefront is continuously connected with the diffracted wave (indicated by td and tdt respectively in the salt and sedimentary layers) generated at the upper corners of the cavity. tt is the direct wave transmitted in the cavity, that propagates downwards. For this wave the cavity acts as a wave-guide, so that much of the energy propagating in the vertical direction remains trapped between the cavity edges and has no lateral radiation. Finally, the weak wavefront td' is the diffraction of the primary wave t generated at the bottom corners of the cavity.

The timings of the main events at normal incidence can be found exactly by looking at the seismograms recorded along the vertical line of receivers (*L1* in Fig. 5a). The transmitted and reflected waves (ttt and ttr respectively) generated at the cavity bottom can be clearly detected at a simulation time of 226 ms (Fig. 4b). The nearly circular wavefront (ttd) which countinously connects ttt and ttr is the diffraction generated by tt at lateral corners of the cavity bottom. At a later time (Fig. 4c), wavefronts ttt and ttd separate from ttr due to the different propagation velo-

[2] Wavefront labels are composed as a string of letters according to the sequence of passages at interfaces; r, t, and d indicate, respectively, reflection, transmission, and diffraction.

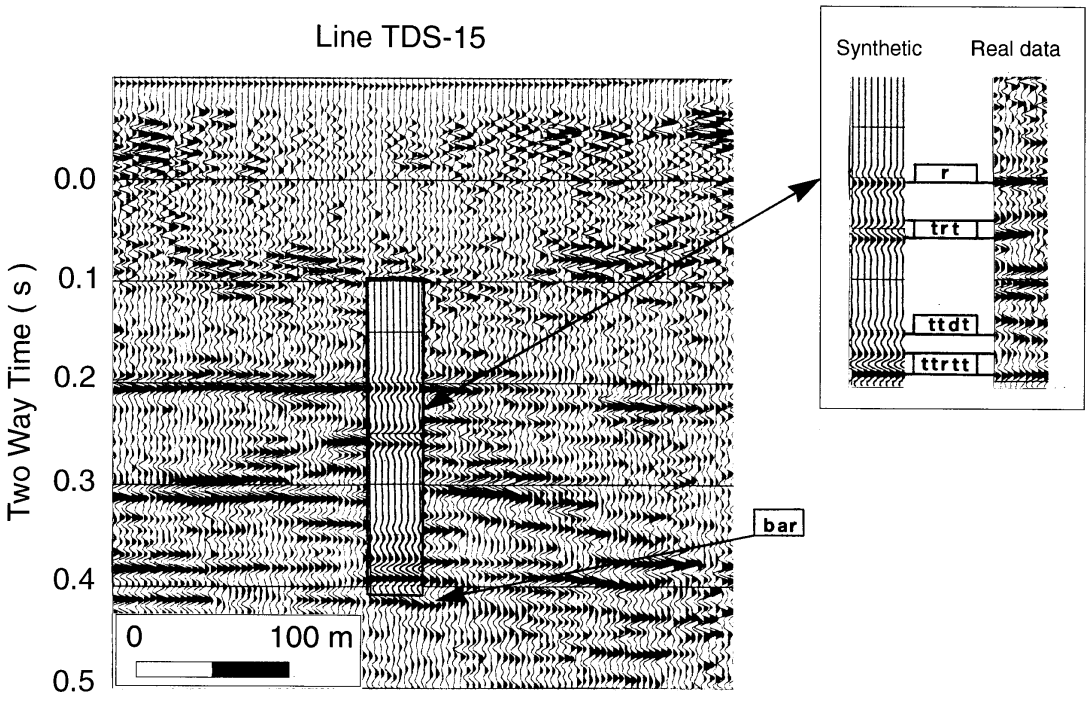

Fig. 7 - Comparison between real (zero-phase stack line TDS-15) and synthetic seismograms. For a better evaluation of the similarity, the synthetic seismogram has been pasted into the real data. The left side of the synthetic display corresponds to the well axis, so that this has to be considered as the models axis of symmetry. The reflector r represents the interface between the sedimentary and salt layers. The reflections trt represent the top cavity reflections (tcr), wich in the real data show the characteristic downward hyperbolic curvature. ttdt represents the diffraction from the walls of the cavity and in the real data cannot be traced confidently. ttrtt represents the bottom cavity reflection (bcr) whose signature fits with real data well . The bar (bottom anhydrite reflector) shows a pull-down below the cavity. This is related to the presence of a low velocity body above the water, filled cavity, which introduces a delay in the arrival time of this reflection.

cities of salt and brine, and generate the nearly circular wavefront which is evident in the figure. Along the vertical axis, the wavefronts t and ttd each have a delay, indicated respectively by *A* and *B* in Fig. 4c; these are not transmitted waves, as one might think at first glance, but are again diffracted events generated respectively at the bottom and top of the cavity.

The propagation eigenmodes of the cavity can be clearly seen within the cavity in all snapshots of Fig. 4. In the last picture, the cavity multiple (ttrr) is propagating downwards. At propagation time 276 ms (Fig. 4d), the cavity bottom diffraction (ttd) enters upwards into the sandstone layer, while the bottom cavity reflection (bcr) (ttrt) reaches the top of the cavity. The two wavefronts (ttd/ttdt and ttrt/ttrtt, respectively in the salt and sandstone layers) are clearly separated and have very different amplitudes, the bcr being much stronger than the diffracted wave. At later propagation times, the upgoing wavefield propagates toward the surface through the sandstone layer, while the first multiple within the cavity give rise to a “replica” of the wavefield, as previously described. In particular, the multiple within the cavity can be clearly seen in

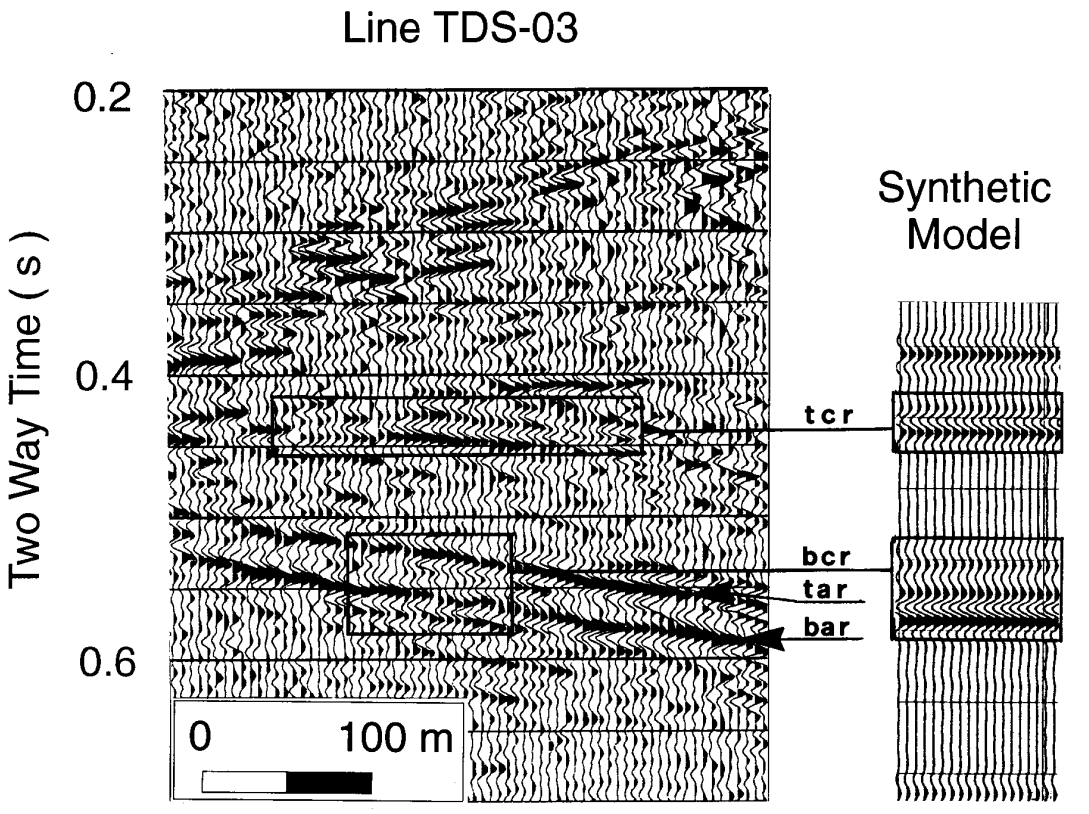

Fig. 8 - Comparison between real (zero, phase stack line TDS-03) and synthetic seismogram computed for the well 28. Even though the synthetic seismogram has been computed with geometrical parameters which do not represent realistically the cavity on this line, the correspondence with the signature from to both top cavity reflector (tcr) and bottom cavity reflector (bcr) is high. In the particular the tcr in the real data maintains the amplitude relationship between the two phases of the wavelet of which it is composed. The bcr identification is not so confident, due to interference between the bcr and the anhydrite layer reflectors (tar and bar). Below the cavity the amplitude of both tar and bar decreases, as expected, owing to the absorption of the seismic signal by the brine.

the vertical profile of Fig. 5a.

Fig. 5b shows the seismic response of the model at the surface (receiver line *L2* in Fig. 3b). The bcr (ttrtt) stands out from all other events, and is characterized by a strong amplitude and curvature. However, it is worth analysing in more detail the differences among the various phases. With respect to the incident wave (Fig. 6), the layer multiple (r) has an amplitude ratio equal to 0.21, and opposite phase; both tcr and bcr (trt and ttrtt, respectively, in the figures) have concordant phase and amplitude ratios of 0.24 and 0.38, respectively. Finally, the top cavity diffraction ttdt has opposite phase and amplitude ratio 0.13. The amplitude of bcr, which is very strong at normal incidence, is highly attenuated at increasing offsets. Thus, the signature of the bcr in a real stacked section is characterized by three main features: (i) a strong curvature, (ii) a reversed phase with respect to the first reflection of the layer, and (iii) an amplitude which is strong at normal incidence but rapidly decays with offset. However, it must be emphasized that these

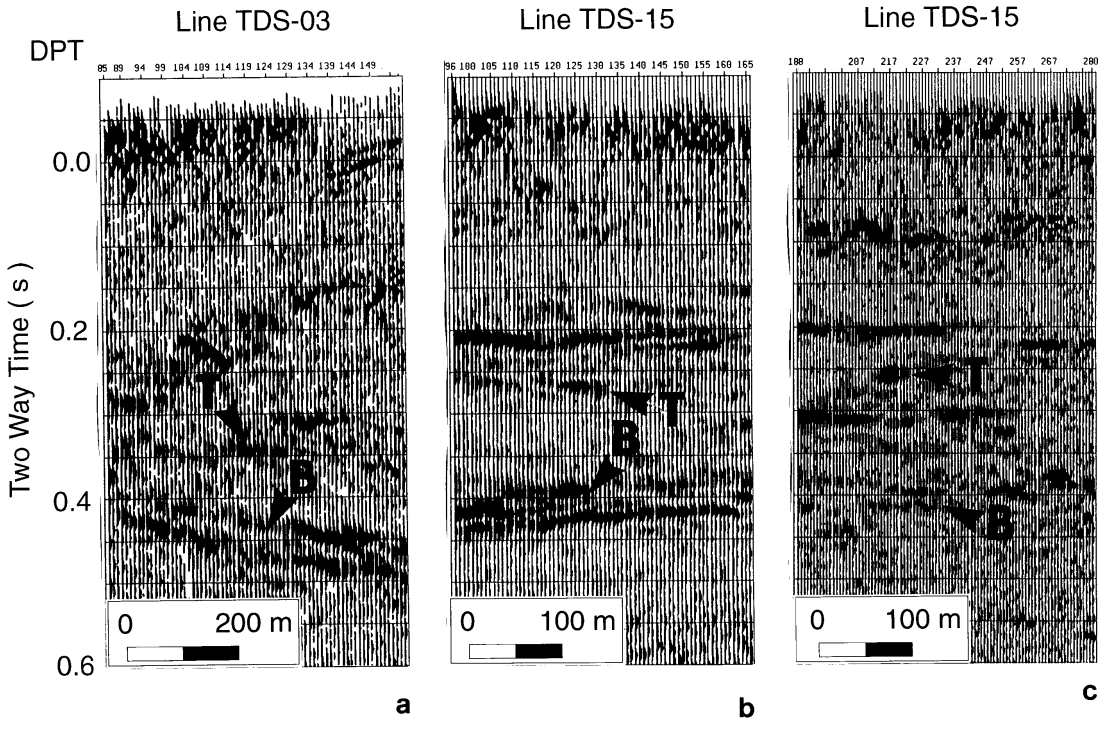

Fig. 9 - Reflection strength (envelope) of the lines TDS-03 (a) and TDS-15 (b,c). T and B indicate the reflections of the cavity top and bottom, respectively. In panels (a) and (c), the bottom reflection is partially masked by the high amplitude reflection of the anhydrite layer. In the panel (b), the amplitude of the bottom reflector is higher than that of the top one, as predicted by the model.

results - in particular (iii) - were obtained with an incident plane wave. The effect would be reduced in a real stacked section, where all but hyperbolic diffractive events are attenuated. Effect (iii) could also be related to energy focusing produced by the concave shape of the cavity bottom. bcr amplification can be clearly identified in real data (Fig. 9b), as described below.

The 2-D (scalar) response differs from a 1-D response obtained for a model corresponding to the velocity profile along the vertical symmetry axis. For instance, we can compare amplitu-

Table 4 - Reflection (r) and transmission (t) coefficients at normal incidence (from medium 1 to 2) at model interfaces.

Medium	**Coefficient**	
1 →2	r	t
SS → SH	0.113	0.887
SH → SS	-0.113	1.113
SH → SW	-0.587	1.587
SW→ SH	0.413	0.587

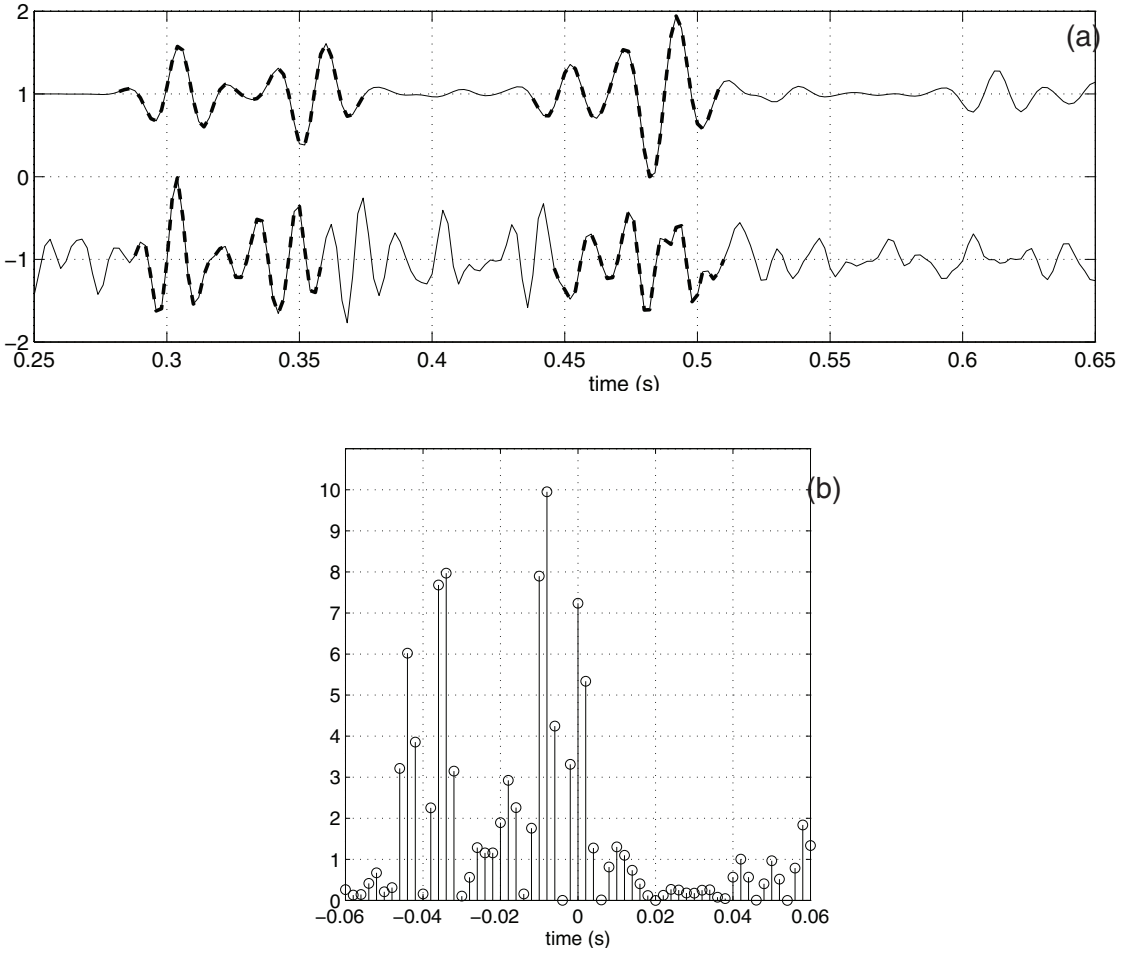

Fig. 10 - Comparison between real (post-stack, line TDS-15) and synthetic seismograms recorded at the surface (receiver R in Fig. 3). (a) Normalized time series. (b) Crosscorrelation (values raised to the power of two) of the two seismograms.

des and phase sign of the main events at the receiver located on the surface along the vertical symmetry axis (R in Fig 3b). Table 4 shows the reflection and transmission coefficients at normal incidence of the three interfaces; they can be used for computing the amplitudes at the surface for more complex events. Values of -0.113, 0.5795, and -0.3798, respectively, are found for the 1-D amplitudes of r, trt, and ttrtt; these amplitudes must be doubled since they refer to a receiver located at the free surface.

The values show some strong discrepancies with respect to those found in the 2-D synthetics. First, the phase sign of bcr obtained in 1-D is opposite to that in 2-D. Moreover, 1-D coefficients predict the highest amplitude for tcr instead of bcr. A plausible explanation for these discrepancies can be found in the 2-D character of the model. For a downgoing wave, cavity top and bottom are convex and concave interfaces, respectively. The former scatters energy outside the cavity, while the latter focuses energy towards the interior of the cavity.

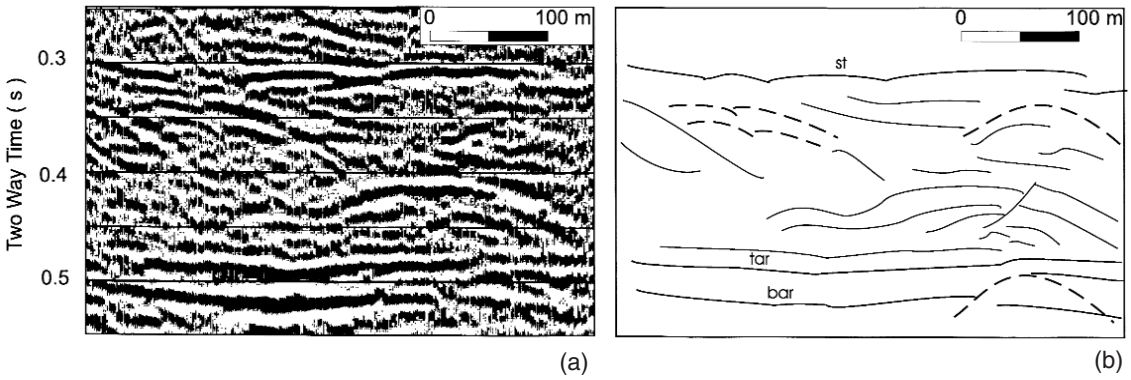

Fig. 11 - Zero-phase stack seismic line TDS-15 (a) and line drawing (b). Continuous and broken lines mark main reflectors and hyperbolic diffractions, respectively. Note that the strong interference between diffractions (due to the cavity) and reflections (due to the geological structure) prevents locating the cavity easily.

Moreover, the bcr upgoing wavefront is further tightened by a bounding effect of the cavity walls. The combined action results in (i) strong reduction of the tcr amplitude, apparently with no phase change, and (ii) bcr amplitude enhancement, probably accompanied by a phase change.

Our synthetics compare fairly well with those obtained by other authors, for instance in the response of an empty cavity computed by Bruno and Rapolla (1997) (see their Fig. 5b). In that case, tcr - in their work called the "cavity diffraction" - is similarly found, although all events due to wave propagation through the cavity are obviously missing. Nevertheless, this comparison emphasizes the difference in response between the two cases: tcr is the only signature of an empty cavity, whilst bcr may be the dominant signature of a cavity filled by some material, especially when the acoustic impedance contrast of this material with respect of the surroundings is high.

4.3. Cavity signature in real data

The cavity response in real data has been accurately analyzed and verified on the basis of the modelling results. This procedure allowed us both to verify the model and to identify the cavities along the seismic sections.

As the first step we chose for comparison the portion of the seismic line at receiver line L2 in Fig. 3b. The real and synthetic seismograms display close similarity; the position of the modelled reflectors, as well as the "diffractive" shape of the tcr (trt) and the bcr (ttrtt), coincide with those present in the real data (Fig. 7). In addition, the reflections related to the anhydrite layer suffer a "pull-down" effect due to the presence of the brine-filled cavity above it (see Fig. 7).

Moreover, all events generated by reflectors located below the cavity suffer strong amplitude decay (Fig. 8). Modelling clearly shows that this loss of energy by the primary waves is due to conversion into reflections and diffractions during propagation through the cavity.

In real data (Fig. 11), signals related to the cavity interfere with those related to the geological structure. The presence of inhomogeneties and deformations in the salt layer makes it difficult to identify the hyperbolic diffractions related to the cavity.

In the following, we shall directly compare real stacked data and synthetic data. However, some observations should be made in advance. The real amplitude of the signals through the cavity is definitely lost during application of the gain recovery function, as computed for the whole seismic survey. Concerning the phase, the strong distortion observable in real data should be, in principle, reduced by conversion to zero-phase, although to do this we must assume that the original wavelet is minimum-phase, a condition not necessarily satisfied.

To overcome these problems and enhance the interpretation, we used reflection strength as a seismic attribute, that is to say the amplitude of the envelope, which is phase-independent and remains associated with major lithologic changes. This was computed by a complex trace analysis technique (Taner, 1979), and allowed us to clearly identify the cavity signature in three different cases (Fig. 9a,b,c). The envelope amplitude ratio between the top and bottom reflectors is maintained whenever the signal is not affected by events related to the geological structure (i.e.: Fig. 9b).

Moreover, the typical diffraction hyperbolae characterizing bcr and tcr in synthetics cannot be easily identified in real data, due to the masking by events related to the geological structures combined with the strong decay with the offset. In addition to the geological “noise”, the hyperbolae can also be confused with others of a structural origin (for instance, inner deformation of the salt layer) (see Fig. 11).

Fig. 10a compares the synthetic and real post-stack seismograms recorded at receiver R of Fig. 3b. Despite the presence of noise and spurious arrivals in the real seismogram, the main events (r, trt, ttdt and ttrtt) can be clearly recognized. Although as already mentioned, amplitudes cannot be strictly compared, the graphical similarity between waveforms is confirmed by the cross-correlation of the two seismograms (Fig. 10b), where a strong peak can be seen at a 0.0 s time-shift. However, the cross-correlation is affected by spurious events that create higher, although physically meaningless, peaks (for instance, at time-shift -0.008 s).

Thus far we have shown that the cavity bottom (bcr) can be clearly seen in the stacked sections, allowing a good estimation of its depth. However, it is hard to claim the same for the top of the cavity (tcr); what seems to be fairly clear in the single trace of Fig. 10a is highly ambiguous in the real stacked section. The presence of high level noise in shallow reflection seismic data (i.e., Fig. 11) is a well known fact (for instance, as documented by Bruno and Rapolla (1997)), and prevents clear identification of the cavity signature with classical seismic processing. A processing technique able to enhance diffraction hyperbolae at the expense of the other events and noise is desirable, but to the authors’ knowledge it has not yet been developed.

From the above discussion it follows that the main dimensions of the cavity can be determined only with very low accuracy by reflection seismics. Nevertheless, high-resolution seismics is the only technique that combines high penetration (say hundreds of metres) with sufficient resolution (within tens of metres). As suggested also by other authors, it would be good practice

to complement very-shallow investigations with other techniques, such as geoelectrics, ground penetrating radar or microgravimetry.

5. Conclusions

Full-wave seismic modelling is a fundamental support tool for interpreting HRS-profiles intended for cavity detection and synthesizing accurately the seismic response of a complex system. A simple 1-D reflection model cannot take into account the whole phenomenon. In the presence of a cavity, wave propagation is characterized by strong diffractions and energy focusing, which introduce new features and change amplitude ratios in seismograms with respect to those obtained by a 1-D model.

When the geologic structure has no strong 3-D character, a simulation with a 2-D model is effective for identifying the cavity signature. In this respect, the image of a cavity in a stacked section is a pair of hyperbolic events, related to the top and bottom of the cavity. If the seismic processing could recover the real amplitude, we would see that the strongest event would be that related to the bottom. In one case, we showed that synthetic seismograms reproduced fairly accurately even real stacked data.

Looking at both simulated and real data, we have shown that the lateral cavity dimension cannot be recovered with the current resolution of a 2-D HRS-survey. Moreover, the heterogeneity of the formations surrounding the cavity generates seismic "noise" that may prevent a clear identification of the cavity signature. However, high-resolution seismics is the only technique that combines high penetration (say hundreds of metres) with sufficient resolution (within tens of metres).

Acknowledgments. This research was partly funded by the European Union (Contract HIRES-SESOM BE5889). The authors would like to thank ing. Lorenzo Musso and dr. Gianfranco Marrazzo of the Montecatini (ITSOS) for their support and contribution. Part of this work was presented at the 59th EAGE Meeting and Technical Exhibition, held in Geneva, Switzerland, on 26-30 May, 1997.

References

Barnes H. L.; 1988: *Ores and minerals*. Open University Press, UK. 181 pp.

Branham K. L. and Steeples D. W.; 1988: *Cavity detection using high resolution seismic reflection methods*. Mining Engineering, **40**, 115-119.

Bruno P. P. G. and Rapolla A.; 1997: *Location of cavities buried in the Neapolitan Yellow Tuff using the seismic reflection method*. Boll. Geof. Teor. Appl., **38**, 25-40.

Miller R. D. and Steeples D. W.; 1995: *Applications of shallow, high-resolution seismic reflection to various mining operations*. Mining Engineering, **47**, 355-361.

Padovani E., Priolo E., and Seriani G.; 1994: *Low- and high-order finite element method: Experience in seismic modeling.* J. Comp. Acoust., **2**, 371-422.

Roda C.; 1964: *Distribuzione e facies dei sedimenti neogeneici del Bacino Crotonese*. Geologia Romana, III, 319-366.

Seriani G. and Priolo E.; 1991: *High-order spectral element method for acoustic wave modeling*. 61th Ann. Int. Mtg., Houston (TX), Soc. Expl. Geophys., Expanded Abstracts, 1561-1564.

Seriani G. and Priolo E.; 1994: *Spectral element method for acoustic wave simulation in heterogeneous media.* Finite Elements in Analysis and Design, **16**, 337-348.

Taner M. T.; 1979: *Complex seismic trace analysis*. Geophysics, **44**, 1041-1063.

Appendix 1 - Chebyshev spectral element method

The Chebyshev spectral element method (SPEM) is a high-order finite element technique, which solves the variational formulation of the differential equation. The computational domain is decomposed into non-overlapping quadrilateral subdomains, and then, on each subdomain, the solution of the variational problem is expressed as a truncated expansion of Chebyshev orthogonal polynomials, as in spectral methods. An investigation of SPEM and its application to the solution of both acoustic and elastic wave equations has been described elsewhere (Seriani and Priolo, 1991; Padovani et al., 1994).

The order of the polynomials is arbitrary, but usually orders six or eight are chosen. The time integration is performed by the implicit Newmark scheme, also called the Constant Average Acceleration, which is a two-step algorithm, unconditionally stable and second order accurate. Analysis of the accuracy was done with numerical experiments in both 1-D and 2-D. The method is, in practice, free of dispersion errors, and the accuracy does not degrade even for very long propagation times. The minimum number G of grid points per wavelength is low: for example, values of $G = 4.5$ and $G = 5.2$ are typically used with polynomial orders $N = 8$ and $N = 6$, respectively, and asymptotically $G = \pi$ for high polynomial orders. Finally, the accuracy does not degrade even for very long propagation times. Material inhomogeneities are modelled simply by defining different material parameters for adjacent elements. The material characteristics do not vary inside the element. At inter-element boundaries, the condition of the displacement continuity is imposed. The free-surface boundary condition is obtained by imposing no constraints at boundary nodes. In inhomogeneous media, SPEM has been shown to be more accurate than other grid methods (Seriani and Priolo, 1994), especially with inclined and curved interfaces, since grid lines can be exactly aligned with material interfaces. These properties of SPEM make it particularly suitable to compute numerically accurate solutions of the full wave equations.